Highly Fluorescent Liquid-Crystalline Dendrimers Based on Borondipyrromethene Dyes

Stéphane Frein,[‡] Franck Camerel,[†] Raymond Ziessel,*[,†] Joaquín Barberá,*[,§] and Robert Deschenaux*[,‡]

[‡]*Institut de Chimie, Université de Neuchâtel, Avenue de Bellevaux 51, Case postale 158, 2009 Neuchâtel, Switzerland,* [†]*Laboratoire de Chimie Organique et Spectroscopies Avancées (LCOSA), CNRS UMR 7515, Université de Strasbourg, Ecole de Chimie, Polymères, Matériaux de Strasbourg (ECPM), 25 rue Becquerel, 67087 Strasbourg, Cedex 02, France, and* [§]*Química Orgánica, Facultad de Ciencias-Instituto de Ciencia de Materiales de Aragón, Universidad de Zaragoza-CSIC, 50009 Zaragoza, Spain*

Fluorescent mesomorphic materials have been synthesized by grafting difluoro-bora-diaza-*s*-indacene (*F*-Bodipy) onto first-, second-, and third-generation liquid-crystalline poly(aryl ester) dendrons functionalized with cyanobiphenyl units. The second- and third-generation dendrimers give rise to smectic A phases; the first-generation dendrimer shows a nematic phase and an unidentified phase. The supramolecular organization within the smectic A phase could be established from X-ray experiments: the dendritic core is oriented approximately parallel to the layer planes and the mesogenic units are oriented perpendicularly above and below the dendritic core; interdigitation occurs between neighboring layers. All the materials are highly fluorescent both in solution and in the mesophases. For the first-generation dendrimer, the formation of *J*-aggregates was detected. The higher-generation dendrons prevented the formation of aggregates. Therefore, the dendrons play the role of liquid-crystalline promoters and protective shells.

Introduction

The chemistry of dendrimers generates a growing interest in materials science[1] and medicinal science.[2] Dendrimers have also been specifically designed to build-up supramolecular architectures, including Langmuir and Langmuir−Blodgett films,[3,4] micelles,[5] membranes,[6] and liquid crystals.[7−13]

Liquid crystals are of interest as they give rise to various mesophases, the properties of which can be used in nano-technologies.[8] In the case of dendrimers, the liquid-crystalline properties can be tuned by careful control of the structure and nature of the mesogenic units (chirality, polarity, length, location) and dendritic core (generation, rigidity/stiffness, connecting groups).[7,9,10,12,13] Furthermore, liquid-crystalline dendrimers tolerate functional groups, so self-assembled functional materials based on such monodispersed macromolecules can be designed. Indeed, we have synthesized liquid-crystalline [60]fullerenes (nematic, chiral nematic, smectic A, smectic C, columnar phases),[11] liquid-crystalline ferrocenes (smectic A phase),[14,15] liquid-crystalline [60]fullerene-ferrocene dyads (smectic A phase),[16,17] and liquid-crystalline diruthenium clusters (nematic and smectic A phases).[18]

On the other hand, highly fluorescent difluoro-bora-diaza-*s*-indacene (*F*-Bodipy) derivatives are a promising class of dyes fulfilling the criteria of stability and chemical availability combined with high molar extinction coefficients, high fluorescence quantum yields, and narrow emission bandwidths in fluid solutions; however, they remain relatively unexplored in the field of liquid-crystalline

*Corresponding authors. E-mail: ziessel@unistra.fr (R.Z.); jbarbera@unizar.es (J.B.); robert.deschenaux@unine.ch (R.D.).
 (1) Tomalia, D. A.; Fréchet, J. M. J. *J. Polym. Sci., Part A: Polym. Chem.* **2002,** *40,* 2719.
 (2) Tekade, R. K.; Kumar, P. V.; Jain, N. K. *Chem. Rev.* **2009,** *109,* 49.
 (3) Cardullo, F.; Diederich, F.; Echegoyen, L.; Habicher, T.; Jayaraman, N.; Leblanc, R. M.; Stoddart, J. F.; Wang, S. *Langmuir* **1998,** *14,* 1955.
 (4) Nierengarten, J.-F.; Eckert, J.-F.; Rio, Y.; del Pilar Carreon, M.; Gallani, J.-L.; Guillon, D. *J. Am. Chem. Soc.* **2001,** *123,* 9743.
 (5) Burghardt, S.; Hirsch, A.; Schade, B.; Ludwig, K.; Böttcher, C. *Angew. Chem., Int. Ed.* **2005,** *44,* 2976.
 (6) Brettreich, M.; Burghardt, S.; Böttcher, C.; Bayerl, T.; Bayerl, S.; Hirsch, A. *Angew. Chem., Int. Ed.* **2000,** *39,* 1845.
 (7) Saez, I. M.; Goodby, J. W. *J. Mater. Chem.* **2005,** *15,* 26.
 (8) Kato, T.; Mizoshita, N.; Kishimoto, K. *Angew. Chem., Int. Ed.* **2006,** *45,* 38.
 (9) Donnio, B.; Guillon, D. *Adv. Polym. Sci.* **2006,** *201,* 45.
(10) Donnio, B.; Buathong, S.; Bury, I.; Guillon, D. *Chem. Soc. Rev.* **2007,** *36,* 1495.
(11) Deschenaux, R.; Donnio, B.; Guillon, D. *New J. Chem.* **2007,** *31,* 1064.
(12) Saez, I. M.; Goodby, J. W. *Struct. Bonding (Berlin)* **2008,** *128,* 1.
(13) Goodby, J. W.; Saez, I. M.; Cowling, S. J.; Görtz, V.; Draper, M.; Hall, A. W.; Sia, S.; Cosquer, G.; Lee, S.-E.; Raynes, E. P. *Angew. Chem., Int. Ed.* **2008,** *47,* 2754.

(14) Deschenaux, R.; Serrano, E.; Levelut, A.-M. *Chem. Commun.* **1997,** 1577.
(15) Chuard, T.; Deschenaux, R. *Chimia* **2003,** *57,* 597.
(16) Campidelli, S.; Vázquez, E.; Milic, D.; Prato, M.; Barberá, J.; Guldi, D. M.; Marcaccio, M.; Paolucci, D.; Paolucci, F.; Deschenaux, R. *J. Mater. Chem.* **2004,** *14,* 1266.
(17) Campidelli, S.; Séverac, M.; Scanu, D.; Deschenaux, R.; Vázquez, E.; Milic, D.; Prato, M.; Carano, M.; Marcaccio, M.; Paolucci, F.; Aminur Rahman, G. M.; Guldi, D. M. *J. Mater. Chem.* **2008,** *18,* 1504.
(18) Frein, S.; Auzias, M.; Sondenecker, A.; Vieille-Petit, L.; Guintchin, B.; Maringa, N.; Süss-Fink, G.; Barberá, J.; Deschenaux, R. *Chem. Mater.* **2008,** *20,* 1340.

materials.[19−21] These dyes are characterized by a pronounced chemical and photochemical stability in solution and in the solid state and by remarkable electron transfer properties. The optical properties are sensitive to modifications of the pyrrole core,[22−24] the central *meso*-position,[25,26] and the boron substituents.[27] They are currently used as chromogenic probes and fluorescent chemosensors,[28−33] fluorescent switches,[34] electro-chemiluminescent materials,[35−37] laser dyes,[38,39] fluorescent labels for biomolecules and cellular imaging,[27] drug delivery agents,[40] photodynamic therapy,[41] and electron-transfer probes for radical ion pairs generated by local electric fields.[42] Such dyes were also used in energy conversion devices such as OLEDs[43] and solar cells.[44−48] These fascinating applications attest to the exceptional robustness and processability of these nonionic dyes allowing their sublimation under high vacuum to provide electroluminescent layers.[36,37]

However, a frequently encountered deficiency in the use of Bodipy in photon or electron responsiveness molecular devices is the difficulty to organize these dyes into predictable assemblies such as liquid-crystalline materials or supramolecular gels. We discovered that amphipathic alkoxydiacylamido platforms bearing chelating

oligopyridine cores[49,50] or *F*-Bodipy dyes[51,52] are able to self-assemble into columnar phases and fibrous networks by means of intermolecular hydrogen bonds. Note that negatively charged Bodipy luminophores also provide columnar phases by ionic self-assembled processes with ammonium-based amphiphiles.[53] Along these lines other luminescent metallomesogens based on d-block transition metals[54−61] or lanthanides[62,63] have previously been studied.

To further explore the possibility to design liquid-crystalline *F*-Bodipy dyes which self-assemble into predictable mesophases, we decided to use mesomorphic dendrimers as liquid-crystalline promoters. Indeed, the latter have been used to synthesize liquid-crystalline materials from bulky, nonmesomorphic units (fullerene, ferrocene, organometallic clusters) as mentioned above. We anticipated that they should also tolerate the *F*-Bodipy unit.

We demonstrate, herein, that a Bodipy framework adequately functionalized with an amino function provides a unique platform to be cross-coupled to liquid-crystalline dendrons and to study the luminescence properties in the mesomorphic materials. In this first study, we selected poly(aryl ester) dendrons carrying cyanobiphenyl mesogenic units to obtain lamellar organization.[11]

Results and Discussion

Materials and Syntheses. The dendritic poly(aryl ester) carboxylic acids **Acid-G₁** (first generation), **Acid-G₂** (second generation), and **Acid-G₃** (third generation) (Chart 1) are obtained in good yields by the oxidation of the corresponding aldehydes[64] with sodium chlorite and sulfamic acid in aqueous tetrahydrofuran (THF). The syntheses of **Acid-G₁**,[65] **Acid-G₂**,[66] and **Acid-G₃**[18] have already been described.

(19) Ulrich, G.; Ziessel, R.; Harriman, A. *Angew. Chem., Int. Ed.* **2008**, *47*, 1184.
(20) Ziessel, R.; Ulrich, G.; Harriman, A. *New J. Chem.* **2007**, *31*, 496.
(21) Loudet, A.; Burgess, K. *Chem. Rev.* **2007**, *107*, 4891.
(22) Haugland, R. P.; Kang, H. C. U.S. Patent 4,774,339, **1998**.
(23) Kollmannsberger, M.; Rurack, K.; Resch-Genger, U.; Daub, J. *J. Phys. Chem. A* **1998**, *102*, 10211.
(24) Burghart, A.; Kim, H.; Wech, M. B.; Thoresen, L. H.; Reibenspies, J.; Burgess, K. *J. Org. Chem.* **1999**, *64*, 7813.
(25) Goze, C.; Ulrich, G.; Charbonnière, L.; Cesario, M.; Prangé, T.; Ziessel, R. *Chem.—Eur. J.* **2003**, *9*, 3748.
(26) Ulrich, G.; Ziessel, R. *J. Org. Chem.* **2004**, *69*, 2070.
(27) Ulrich, G.; Goze, C.; Guardigli, M.; Roda, A.; Ziessel, R. *Angew. Chem., Int. Ed.* **2005**, *44*, 3694.
(28) Wagner, R. W.; Lindsey, J. S. *Pure Appl. Chem.* **1996**, *68*, 1373.
(29) Beer, G.; Daub, J.; Rurack, K. *Chem. Commun.* **2001**, 1138.
(30) Turfan, B.; Akkaya, E. U. *Org. Lett.* **2002**, *4*, 2857.
(31) Beer, G.; Niederalt, C.; Grimme, S.; Daub, J. *Angew. Chem., Int. Ed.* **2000**, *39*, 3252.
(32) Kollmannsberger, M.; Rurack, K.; Resch-Genger, U.; Rettig, W.; Daub, J. *Chem. Phys. Lett.* **2000**, *329*, 363.
(33) Sancenón, F.; Martínez-Máñez, R.; Soto, J. *Angew. Chem., Int. Ed.* **2002**, *41*, 1416.
(34) Golovkova, T. A.; Kozlov, D. V.; Neckers, D. C. *J. Org. Chem.* **2005**, *70*, 5545.
(35) Lai, R. Y.; Bard, A. J. *J. Phys. Chem. B* **2003**, *107*, 5036.
(36) Brom, J. M.; Langer, J. L. *J. Alloys Compd.* **2002**, *338*, 112.
(37) Hepp, A.; Ulrich, G.; Schmechel, R.; von Seggern, H.; Ziessel, R. *Synth. Met.* **2004**, *146*, 11.
(38) Chen, T.; Boyer, J. H.; Trudell, M. L. *Heteroat. Chem.* **1997**, *8*, 51.
(39) Sathyamoorthi, G.; Wolford, L. T.; Haag, A. M.; Boyer, J. H. *Heteroat. Chem.* **1994**, *5*, 245.
(40) McCusker, C.; Carroll, J. B.; Rotello, V. M. *Chem. Commun.* **2005**, 996.
(41) Atilgan, S.; Ekmekci, Z.; Dogan, A. L.; Guc, D.; Akkaya, E. U. *Chem. Commun.* **2006**, 4398.
(42) Debreczeny, M. P.; Svec, W. A.; Wasielewski, M. R. *Science* **1996**, *274*, 584.
(43) Bonardi, L.; Kanaan, H.; Camerel, F.; Jolinat, P.; Retailleau, P.; Ziessel, R. *Adv. Funct. Mater.* **2008**, *18*, 401.
(44) Erten-Ela, S.; Yilmaz, M. D.; Icli, B.; Dede, Y.; Icli, S.; Akkaya, E. U. *Org. Lett.* **2008**, *10*, 3299.
(45) Rousseau, T.; Cravino, A.; Bura, T.; Ulrich, G.; Ziessel, R.; Roncali, J. *Chem. Commun.* **2009**, 1673.
(46) Kumaresan, D.; Thummel, R. P.; Bura, T.; Ulrich, G.; Ziessel, R. *Chem.—Eur. J.* **2009**, *15*, 6335.
(47) Hattori, S.; Ohkubo, K.; Urano, Y.; Sunahara, H.; Nagano, T.; Wada, Y.; Tkachenko, N. V.; Lemmetyinen, H.; Fukuzumi, S. *J. Phys. Chem. B* **2005**, *109*, 15368.
(48) Rousseau, T.; Cravino, A.; Bura, T.; Ulrich, G.; Ziessel, R.; Roncali, J. *J. Mater. Chem.* **2009**, *19*, 2298.

(49) Camerel, F.; Ulrich, G.; Ziessel, R. *Org. Lett.* **2004**, *6*, 4171.
(50) Ziessel, R.; Pickaert, G.; Camerel, F.; Donnio, B.; Guillon, D.; Cesario, M.; Prangé, T. *J. Am. Chem. Soc.* **2004**, *126*, 12403.
(51) Camerel, F.; Bonardi, L.; Schmutz, M.; Ziessel, R. *J. Am. Chem. Soc.* **2006**, *128*, 4548.
(52) Camerel, F.; Bonardi, L.; Ulrich, G.; Charbonnière, L.; Donnio, B.; Bourgogne, C.; Guillon, D.; Retailleau, P.; Ziessel, R. *Chem. Mater.* **2006**, *18*, 5009.
(53) Camerel, F.; Ulrich, G.; Barberá, J.; Ziessel, R. *Chem.—Eur. J.* **2007**, *13*, 2189.
(54) Bayón, R.; Coco, S.; Espinet, P. *Chem.—Eur. J.* **2005**, *11*, 1079.
(55) Arias, J.; Bardají, M.; Espinet, P. *Inorg. Chem.* **2008**, *47*, 3559.
(56) Cavero, E.; Uriel, S.; Romero, P.; Serrano, J. L.; Giménez, R. *J. Am. Chem. Soc.* **2007**, *129*, 11608.
(57) Kishimura, A.; Yamashita, T.; Yamaguchi, K.; Aida, T. *Nat. Mater.* **2005**, *4*, 546.
(58) Camerel, F.; Ziessel, R.; Donnio, B.; Bourgogne, C.; Guillon, D.; Schmutz, M.; Iacovita, C.; Bucher, J.-P. *Angew. Chem., Int. Ed.* **2007**, *46*, 2659.
(59) Ghedini, M.; Pucci, D.; Crispini, A.; Bellusci, A.; La Deda, M.; Aiello, I.; Pugliese, T. *Inorg. Chem. Commun.* **2007**, *10*, 243.
(60) Cardolaccia, T.; Li, Y.; Schanze, K. S. *J. Am. Chem. Soc.* **2008**, *130*, 2535.
(61) Kozhevnikov, V. N.; Donnio, B.; Bruce, D. W. *Angew. Chem., Int. Ed.* **2008**, *47*, 6286.
(62) Binnemans, K. *J. Mater. Chem.* **2009**, *19*, 448.
(63) Terazzi, E.; Suarez, S.; Torelli, S.; Nozary, H.; Imbert, D.; Mamula, O.; Rivera, J.-P.; Guillet, E.; Bénech, J.-M.; Bernardinelli, G.; Scopelliti, R.; Donnio, B.; Guillon, D.; Bünzli, J.-C. G.; Piguet, C. *Adv. Funct. Mater.* **2006**, *16*, 157.
(64) Campidelli, S.; Lenoble, J.; Barberá, J.; Paolucci, F.; Marcaccio, M.; Paolucci, D.; Deschenaux, R. *Macromolecules* **2005**, *38*, 7915.
(65) Terazzi, E.; Bocquet, B.; Campidelli, S.; Donnio, B.; Guillon, D.; Deschenaux, R.; Piguet, C. *Chem. Commun.* **2006**, 2922.
(66) Campidelli, S.; Vázquez, E.; Milic, D.; Lenoble, J.; Atienza Castellanos, C.; Sarova, G.; Guldi, D. M.; Deschenaux, R.; Prato, M. *J. Org. Chem.* **2006**, *71*, 7603.

Chart 1

Acid-G$_1$

Acid-G$_2$

R = —(CH$_2$)$_{10}$—O—⬡—CO$_2$—⬡—⬡—CN
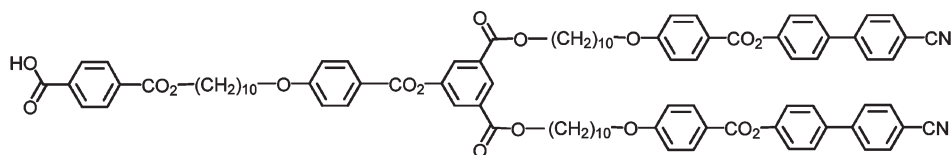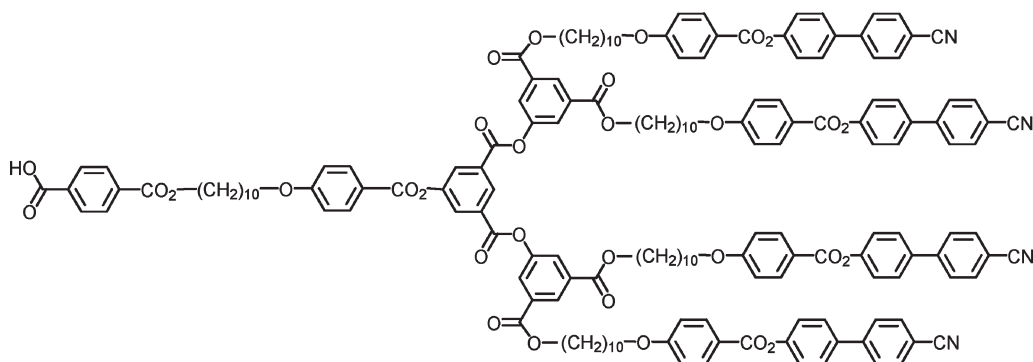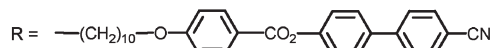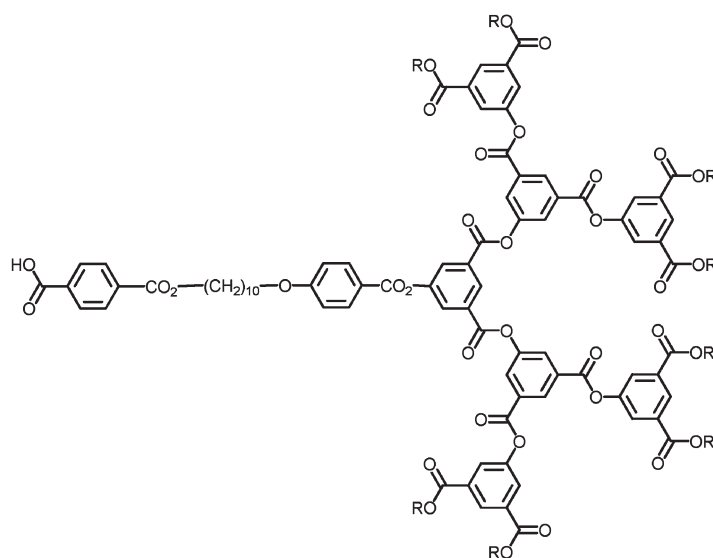
Acid-G$_3$

The synthesis of the **BOD-G$_n$** ($n = 1, 2, 3$) compounds (Chart 2) was inspired by peptide synthesis[67] and was made feasible by using a solution of the **Acid-G$_n$** dendrimers and a Bodipy amino derivative[68] in the presence of the hydrochloride salt of 1-ethyl-3-[3-(dimethylamino)-propyl]carbodiimide (EDC·HCl) and 4-dimethylamino-pyridine (DMAP) (Scheme 1).

The purification of the **BOD-G$_n$** materials was achieved by column chromatography on silica gel followed by crystallization from a CH$_2$Cl$_2$/CH$_3$CN mixture. The molecular structures and purity were assigned by

^{1}H and ^{13}C NMR spectroscopy, infrared spectroscopy, mass spectrometry, and elemental analysis.

Liquid-Crystalline Properties. The thermal and liquid-crystalline properties of **BOD-G$_n$** were investigated by polarized optical microscopy (POM) and differential scanning calorimetry (DSC). The mesomorphic properties of **Acid-G$_n$** have already been described elsewhere.[18,65,66] The phase transition temperatures and thermodynamic data are reported in Table 1.

Compound **BOD-G$_1$** shows two mesophases, a nematic phase (schlieren texture) and a mesophase that could not be identified by POM as no typical texture was observed. Compounds **BOD-G$_2$** and **BOD-G$_3$** lead to the formation of smectic A phases (focal-conic and homeotropic textures).

(67) Chini, M.; Crotti, P.; Macchia, F. *Tetrahedron Lett.* **1990**, *31*, 4661.
(68) Ziessel, R.; Bonardi, L.; Retailleau, P.; Ulrich, G. *J. Org. Chem.* **2006**, *71*, 3093.

Chart 2

BOD-G₁

BOD-G₂
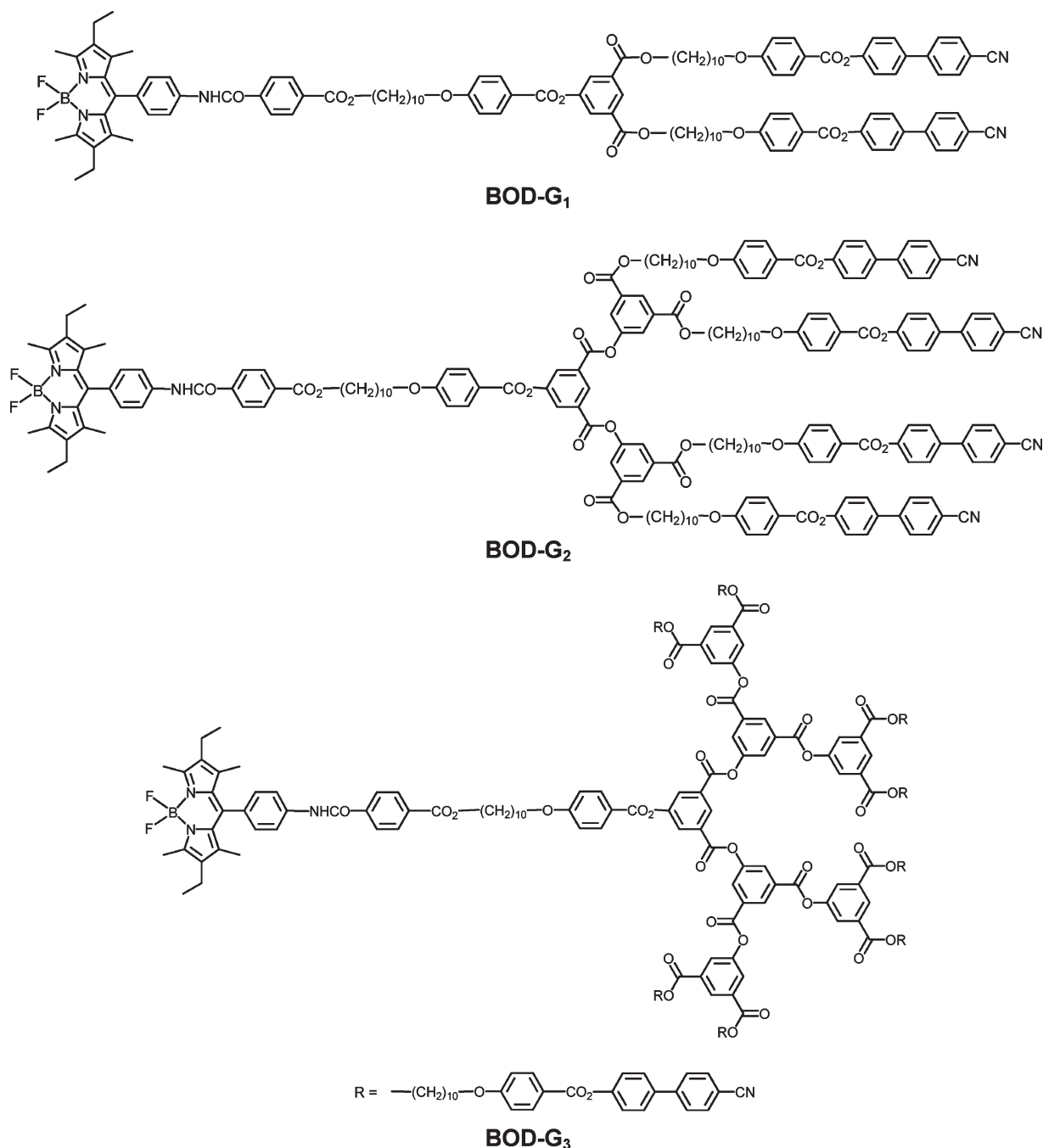
BOD-G₃

The textures of the nematic and smectic A phases displayed by **BOD-G$_1$** and **BOD-G$_3$** are shown in Figures 1 and 2, as illustrative examples. The clearing point increases with the dendrimer generation. This behavior is due to the fact that the intermolecular interactions increase with the number of cyanobiphenyl units. A lowering of the clearing point is observed for the **BOD-G$_n$** compounds compared to their corresponding **Acid-G$_n$** precursors. This is a consequence of the presence of the *F*-Bodipy unit which generates steric hindrance, probed by the tetrahedric boron atom and the orthogonality of the phenyl ring in the meso position, the consequence of which is a decrease of the intermolecular interactions. Finally, the formation of smectic A phases observed for

BOD-G$_2$ and **BOD-G$_3$** (and also for the liquid-crystalline precursors **Acid-G$_2$** and **Acid-G$_3$**) is in agreement with the nature of the dendromesogens which have a strong tendency to align parallel one to each other and so give rise to the formation of layers, as observed for analogous liquid-crystalline dendrimers[11,16−18] and side-chain liquid-crystalline polymers.[69−71]

Supramolecular Organization. The structures of the mesophases displayed by the **BOD-G$_n$** compounds were

(69) Kawakami, T.; Kato, T. *Macromolecules* **1998**, *31*, 4475.
(70) Yamada, M.; Itoh, T.; Nakagawa, R.; Hirao, A.; Nakahama, S.-i.; Watanabe, J. *Macromolecules* **1999**, *32*, 282.
(71) Barmatov, E. B.; Filippov, A. P.; Shibaev, V. P. *Liq. Cryst.* **2001**, *28*, 511.

Scheme 1. [a]
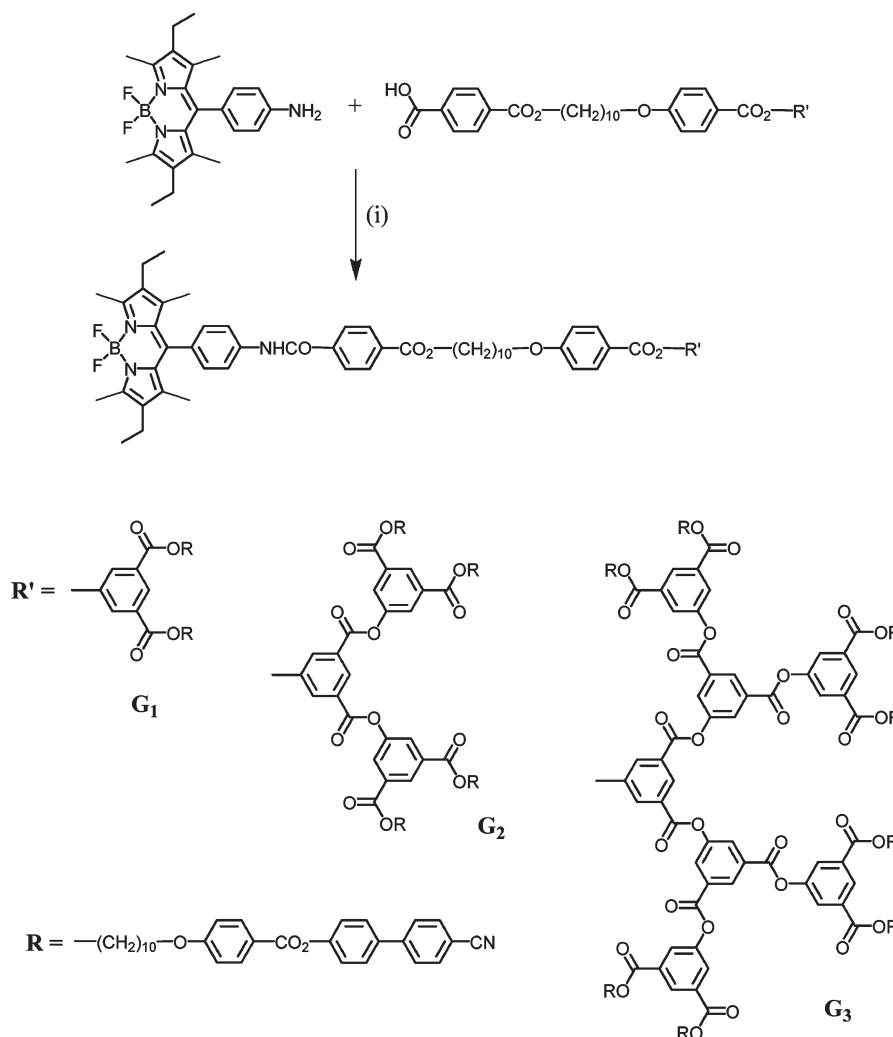
[a] (i) 1-Ethyl-3-[3-(dimethylamino)propyl]carbodiimide (EDC·HCl), 4-dimethylamino-pyridine (DMAP), CH_2Cl_2, r.t.; yields: 57% for **BOD-G$_1$**, 56% for **BOD-G$_2$**, 61% for **BOD-G$_3$**.

Table 1. Phase-Transition Temperatures[a] with Enthalpy Changes for the BOD-G$_n$ Dendrimers and Their Dendritic Carboxylic Acid Precursors

compound	T_g (°C)	transition	T (°C)	ΔH (kJ mol^{-1})	ΔH (kJ mol^{-1}) per mesogenic unit
Acid-G$_1$[65]		Cr → N	39	1.9	0.95
		N → I	194	6.2	3.1
Acid-G$_2$[66]	45	SmA → I	203	18.6	4.65
Acid-G$_3$[18]	55	SmA → I	227	40.9[b]	5.1
BOD-G$_1$	45	Cr → M[c]	86	41.0	20.5
		M → N	119	0.2	0.1
		N → I	123	0.1	0.05
BOD-G$_2$	72	Cr → SmA[c]	100	60.1	15.0
		SmA → I	155	8.3	2.1
BOD-G$_3$	54	Cr → SmA[c]	83	67.8	8.5
		SmA → I	210	37.0	4.6

[a] T_g: glass transition temperature; Cr = semicrystalline solid; SmA = smectic A phase; N = nematic phase; M = unidentified mesophase; I = isotropic liquid. Temperatures are given as the onset of the peaks obtained during the second heating run. [b] A value of 4.9 kJ mol^{-1} was incorrectly reported in ref 18. [c] Determined during the first heating run.

investigated by X-ray diffraction (XRD) at variable temperatures. The XRD data are reported in Table 2. At room temperature, before any thermal treatment, the three compounds yield patterns typical of crystalline phases. When they are heated into the mesophases and cooled down to room temperature, the XRD measurements indicate that crystallization does not take place and

the mesomorphic order is maintained. This result is consistent with the POM observations and DSC curves (as an illustrative example, DSC curves of **BOD-G$_3$** are shown in Figure 3). For **BOD-G$_3$**, the diffraction patterns taken under these conditions are characteristic of a smectic phase (Figure 4). They contain a sharp, strong reflection in the small-angle region and a broad, diffuse
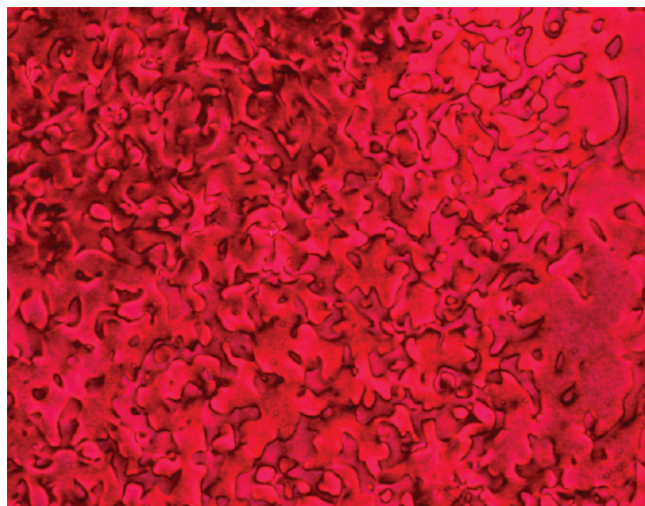
Figure 1. Thermal optical micrograph of the schlieren texture displayed by **BOD-G₁** in the nematic phase at 131 °C.

Figure 2. Thermal optical micrograph of the focal−conic fan texture displayed by **BOD-G₃** in the smectic A phase at 161 °C.

Table 2. X-ray Data of the BOD-Gₙ Dendrimers in the Smectic A Phase

compound	T (°C)	$d_{002} \pm 0.5$ Å	d-layer spacing ± 1 Å
BOD-G₂	105	24	48
BOD-G₃	25	25.5	51
	105	25	50
	155	24.5	49
	205	24	48

halo in the wide-angle region. The small-angle maximum arises from the reflection of the X-rays on the smectic planes and, by applying Bragg's law, this maximum gives a d-layer spacing of 25.5 Å. The halo is consistent with the absence of positional order inside the layers. Thus, the pattern corresponds to a disordered smectic phase, that is, a smectic A phase in agreement with the textures observed by POM. The measurements were performed at several temperatures between the melting transition, detected during the first heating run by DSC, and the clearing point. In all cases, the same type of diffractograms was qualitatively obtained. The measured d-layer spacings slightly decreased upon increasing the temperature.
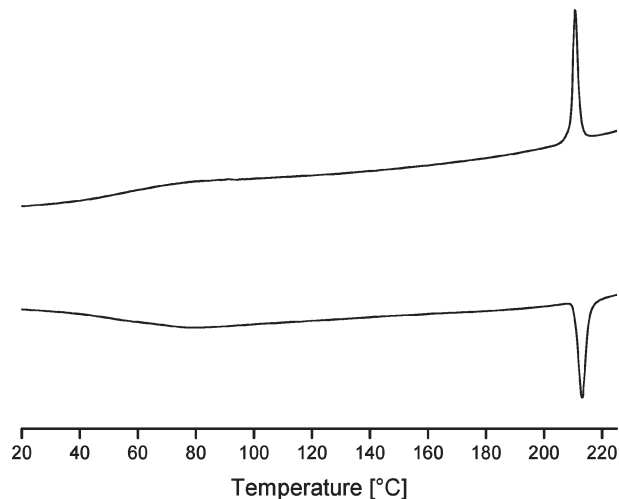

Figure 3. Differential scanning thermograms of **BOD-G₃** registered during the second heating (bottom)−cooling (top) cycle.
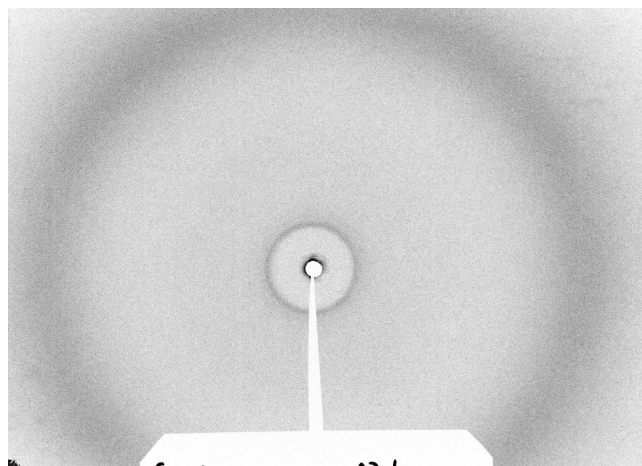

Figure 4. Small-angle diffraction pattern of compound **BOD-G₃** in the smectic A phase at room temperature (the sample was heated into the isotropic fluid and cooled down to room temperature).

The d-values obtained are 25, 24.5, and 24 Å at 105, 155, and 205 °C, respectively.

For **BOD-G₂**, a diffraction pattern typical of a smectic phase was obtained when the sample was heated above the clearing point and then cooled down to the mesophase, at 105 °C in this case. Under these conditions, a pattern similar to those recorded for **BOD-G₃** was obtained. The d-layer spacing was found to be 24 Å. From this value, which is close to the one obtained for **BOD-G₃**, it is concluded that both **BOD-G₂** and **BOD-G₃** display the same type of mesophases. It is interesting to note that the intensity of the Bragg reflection for **BOD-G₂** is much weaker and broader than for **BOD-G₃**.

For **BOD-G₁**, no reflections could be detected under any conditions applied from the clearing point down to room temperature. This result is consistent with the nematic phase identified by POM. However, both DSC and POM techniques indicated the transformation of the nematic phase into another one at 119 °C. Considering the structure of the liquid-crystalline promoters, this mesophase should be a disordered smectic phase.
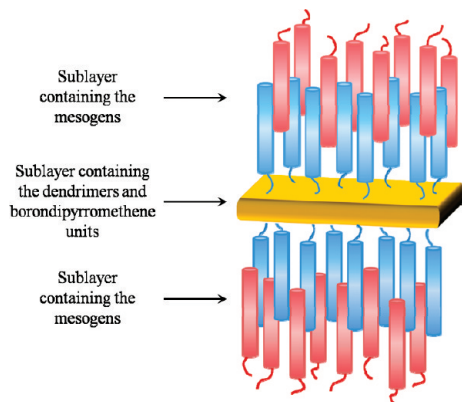
Figure 5. Postulated supramolecular organization of **BOD-G₃** within the smectic A phase. The interdigitation is illustrated by the red and blue cyanobiphenyl units: the blue units belong to the dendrimers which are displayed on the drawing, and the red units belong to dendrimers of adjacent layers. Some Bodipy units can also be localized in the sublayers containing the mesogenic units.

The absence of Bragg reflections for the low-temperature mesophase can account for a poor molecular layering due to a diffuse interface between the layers. This interface seems to become more and more diffuse as the generation of the dendrimer decreases, as deduced from the decrease in intensity and broadening of the Bragg signals in **BOD-G₂** compared to **BOD-G₃**, and from the absence of signals in the pattern of **BOD-G₁**.

To understand this behavior, it is important to compare the measured d-layer spacings and the molecular lengths. The estimated molecular lengths L (obtained by Hyper-Chem software) in the most extended conformation are about 79 Å for **BOD-G₂** and 76 Å for **BOD-G₃**; as for the mesogenic unit, including the decamethylene spacer, the molecular length is about 31 Å. It is obvious that the experimentally determined d-layers spacings (i.e., 24 and 25 Å for **BOD-G₂** and **BOD-G₃**, respectively) cannot correspond to the layer thicknesses and thus the Bragg reflections are in fact the second order reflections, the first order reflections being absent. Such a result can be obtained when there is a strong modulation of the electronic density with a periodicity equal to half that of the layer thickness. In this case, the actual d-layer thicknesses at 105 °C are 48 Å (2 × 24 Å) for **BOD-G₂** and 50 Å (2 × 25 Å) for **BOD-G₃**. The fact that d is significantly smaller than L implies that the dendritic core extends laterally, approximately parallel to the layer planes. The cyanobiphenyl mesogenic units are oriented above and below the dendritic core and interdigitation occurs between neighboring layers (Figure 5). This model, which is in agreement with that found for other dendritic systems containing the same mesogenic units,[18,64] implies the presence of a sublayer containing the aromatic dendritic branches located in the middle of the smectic layer. This sublayer has a high electronic density, and thus the smectic layers are formed by two alternating sublayers containing the dendritic core (including the *F*-Bodipy core) and the mesogenic units. This alternating structure accounts for the above-mentioned modulation of the electronic density with a periodicity that is half that

of the layer thickness. This phenomenon has been described for side-chain liquid-crystalline polymers and is accounted by the confinement of the polymer backbones in a thin sublayer perpendicular to the director, so that the backbones (the dendritic core in this case) produce an electron density maximum comparable to that of the mesogenic cores.[72,73] Moreover, the interdigitation of the cyanobiphenyl mesogenic units makes the interface between the layers diffuse, and this is in agreement with the weakness (for **BOD-G₂** and **BOD-G₃**) [or absence (for **BOD-G₁**)] of the small-angle diffraction peaks.

Spectroscopic Studies. Spectroscopic data for the **BOD-Gₙ** compounds are gathered in Table 3. All the compounds show similar absorption features which are characteristic of Bodipy fluorophores, and a typical example is given in Figure 6. The absorption spectrum is composed of a strong $S_0 \rightarrow S_1$ ($\pi \rightarrow \pi^*$) transition located around 525 nm, with molar extinction coefficients ranging from 70 000 to 80 000 M^{-1} cm^{-1}, in keeping with classical *F*-Bodipy derivatives.[68] A second absorption band, centered around 355 nm, is assigned to the $S_0 \rightarrow S_2$ transition of the Bodipy subunit.[74] The third absorption around 275 nm is likely due to $\pi-\pi^*$ and $n-\pi^*$ transitions localized on the dendrimer and dipyrromethene fragments. As expected, the absorption coefficients of the bands centered at 525 and 355 nm, belonging to the dipyrromethene fragment, remain constant within the series, whereas the absorption coefficient of the absorption band centered at 275 nm increases proportionally with the generation of the dendrimer. The **BOD-Gₙ** compounds have high fluorescence quantum yields ranging from 61 to 65%. The weak Stoke shifts (about 500 cm^{-1}) observed over the whole series of fluorophores are in agreement with a weakly polarized excited state typical of singlet emitting state. The excitation spectra, centered on the Bodipy fragment, match the absorption spectra (Figure 6 as a typical example), which is in agreement with a unique excited state. The fluorescence decay profiles of these molecules can be fitted by a single-exponential, with fluorescence lifetimes ranging from 6.1 to 7.7 ns (Table 3), in line with a singlet emissive state. The radiative rate constants are similar for all **BOD-Gₙ** compounds (within experimental error), attesting little influence of the mesogenic platform to the *F*-Bodipy residue.

Temperature-dependent fluorescence measurements were performed in the solid state with a spectrofluorimeter equipped with an optical fiber and a heating stage. The evolution of the luminescence of compound **BOD-G₁** in the solid state as a function of the temperature is presented in Figure 7. The emission spectrum measured at room temperature shows a large emission band from 525 up to 700 nm with two distinct maxima at 565 and

(72) Davidson, P.; Levelut, A. M.; Achard, M. F.; Hardouin, F. *Liq. Cryst.* **1989**, *4*, 561.
(73) Barberá, J.; Giorgini, L.; Paris, F.; Salatelli, E.; Tejedor, R. M.; Angiolini, L. *Chem.—Eur. J.* **2008**, *14*, 11209.
(74) Karolin, J.; Johansson, L. B.-A.; Strandberg, L.; Ny, T. *J. Am. Chem. Soc.* **1994**, *116*, 7801.

Table 3. Spectroscopic Data of the BOD-G$_n$ Dendrimers Measured in Dichloromethane Solutions at 298 K

	C (mol·L^{-1})	λ_{abs} (nm)	λ (M^{-1}·cm^{-1})	λ_F (nm)	$\Phi_F{}^a$	τ_F (ns)	$k_r{}^b$ (10^8 s^{-1})	$k_{nr}{}^b$ (10^8 s^{-1})
BOD-G$_1$	2.4×10^{-6}	525	72300	540	0.65	6.1	0.90	0.74
		355	11500					
		275	149300					
BOD-G$_2$	1.4×10^{-6}	525	70900	540	0.63	7.7	0.82	0.48
		355	11200					
		275	277500					
BOD-G$_3$	3.0×10^{-7}	525	78900	540	0.61	6.8	0.90	0.57
		355	12300					
		275	603000					

^{a} Determined in dichloromethane solution using Rhodamine 6G as reference ($\Phi_F = 0.78$ in water, $\lambda_{exc} = 488$ nm).[75] All Φ_F are corrected for changes in refractive index. ^{b} Calculated using the following equations: $k_r = \Phi_F/\tau_F$, $k_{nr} = (1 - \Phi_F)/\tau_F$, assuming that the emitting state is produced with unit quantum efficiency.
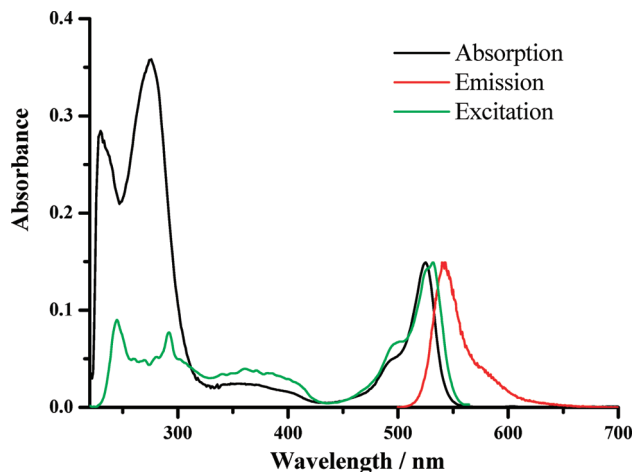

Figure 6. Absorption spectra for **BOD-G$_3$** (absorption in black, excitation in green), and emission spectra in red ($\lambda_{exc} = 490$ nm). All spectra were measured in CH$_2$Cl$_2$ at rt ($c = 2.4 \times 10^{-6}$ M).

650 nm. The band at 565 nm can be attributed, with respect to the measurements performed in dichloromethane, to the emission of the monomeric species and the red-shifted band at 650 nm to the emission of aggregated Bodipy species.[52] This red-shift of the emission maxima is induced by the formation of molecular *J*-aggregates with a head-to-tail arrangement in which the excitonic energy is delocalized as a result of intermolecular coupling between molecules.[21] Upon heating, the intensity of the emission band at 565 nm increases at the expense of the emission band at 650 nm. The augmentation of the temperature likely facilitates the dislocation of the aggregates in favor of the monomeric species which emits at 565 nm. The observed process is completely reversible, and upon cooling, the emission at 565 nm is depleted in favor of the emission at 650 nm.

For the larger **BOD-G$_2$** and **BOD-G$_3$** dendrimers, the room temperature luminescence spectra have a broad emission bands centered at 597 nm and at 604 nm, respectively. This single emission is likely attributed to the emission of the monomeric species, and no evidence for formation of aggregates was observed. Increasing the temperature does not significantly change the shape of the emission band but decreases the emission intensity due to nonradiative deactivation pathways. The emission maxima are slightly blue-shifted upon heating. The shift of the spectrum and the decrease of the intensity evolve mono-
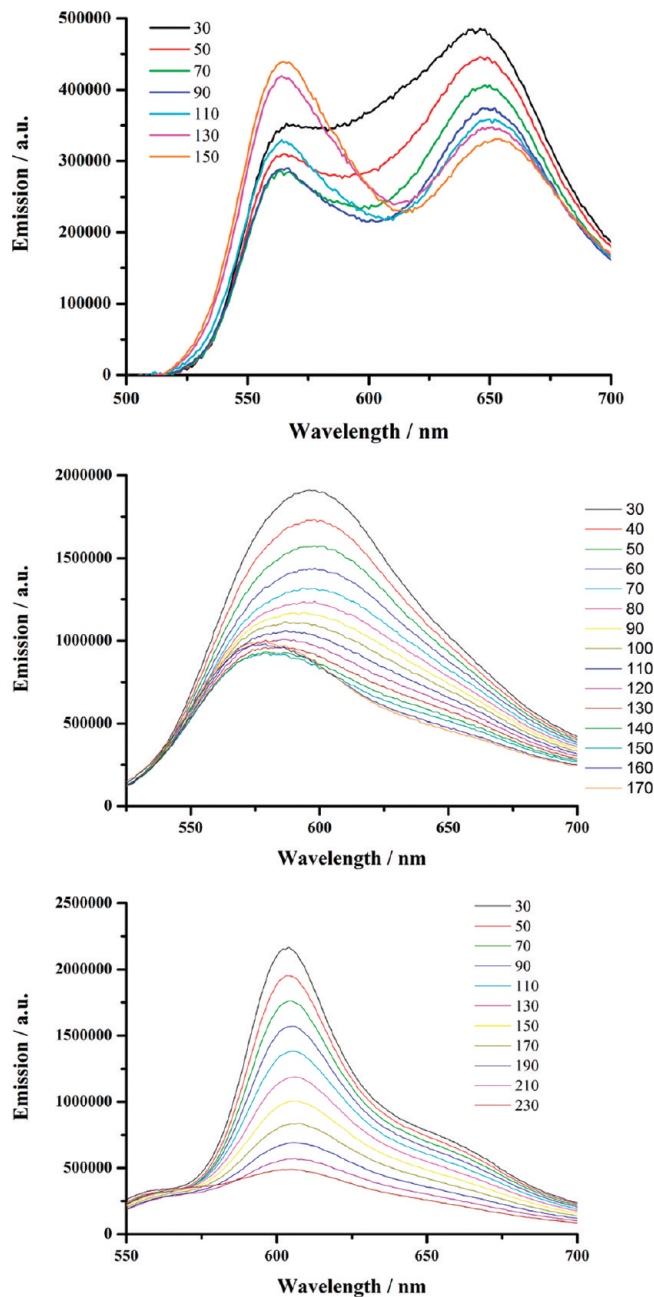

Figure 7. Solid state emission spectra of **BOD-G$_1$** (upper), **BOD-G$_2$** (middle), and **BOD-G$_3$** (lower), measured at various temperatures upon heating ($\lambda_{ex} = 390$ nm) (second heating cycle).

tonically, and the shape of the emission band remains large and unstructured. No clear transitional effect can

be observed above and below the isotropization temperature. Upon cooling, the reverse process is observed in both cases excluding decomposition of the materials. The emission spectrum is gradually red-shifted, and the intensity of emitted light increases, reaching the value of the room temperature.

From these solid-state emission studies, it clearly appears that *F*-Bodipy aggregates are prominently formed with dendrimer G_1 whereas less aggregated species are formed with the larger G_2 and G_3 dendrimers. In the case of G_2 and G_3 dendrimers, their large sizes, most likely, account for a better coating and isolation of the *F*-Bodipy fragment. The smaller size dendrimer appears to be less effective to isolate the Bodipy fluorophores in the mesomorphic state.

Conclusions

Difluoro-bora-diaza-*s*-indacene dyes have been successfully grafted onto poly(aryl ester) dendrons bearing cyanobiphenyl mesogenic units *via* the formation of amide bonds. These dual dendritic units appear remarkably stable in solution and in the solid state, and no fluorescence decrease was observed versus time even by heating up to 200 °C. The second- and third-generation dendrimers display smectic A phases; the first-generation dendrimer shows a nematic phase and an unidentified phase. Interestingly, we found that the dyes remain highly fluorescent in the mesophases. Moreover, aggregates of *F*-Bodipy are prominently present in the first-generation dendrimer and the second- and third-generation dendrimers favor dispersion of the dye moieties, preventing the formation of aggregates. The red shift of the emitted light above 700 nm is in favor of *J*-aggregates. Our results show that highly fluorescent dendritic mesomorphic materials can be adequately produced and that the aggregation tendency of *F*-Bodipy can be adjusted by the choice of the dendrimer generation. We believe that this research is helpful for the design of multicolored liquid crystals for which adequate mixing of mesogenic dyes with different colors might favor excitonic energy transfer processes strongly dependent on the nature of the mesophases. Even though a significant amount of knowledge is available in the design of fluorescent mesogens, the control of energy transfer processes in a few nanometers scale length and their application in organic electronic devices are still challenges, in particular within the context of the emerging areas of supramolecular electronics and nanodevices.

Experimental part

Transition temperatures (onset point) and enthalpies were determined with a differential scanning Mettler DSC DSC822^e calorimeter, under N₂/He, at a rate of 10 °C/min. Optical studies were conducted using a Zeiss-Axioskop polarizing microscope equipped with a Linkam-THMS-600 variable-temperature stage. The XRD patterns were obtained with a pinhole camera (Anton-Paar) operating with a point-focused Ni-filtered Cu Kα beam. The samples were held in Lindemann glass

(75) Olmsted, J. *J. Phys. Chem.* **1979**, *83*, 2581.

capillaries (1 mm diameter) located perpendicular to the X-ray beam and heated, when necessary, with a variable-temperature attachment. The patterns were collected on flat photographic film perpendicular to the X-ray beam. The *d*-layer spacings were obtained via Bragg's law.

The 300.1 (¹H) and 75.5 MHz (¹³C) spectra were recorded at room temperature using perdeuterated solvents as internal standards. FT-IR spectra were recorded using a Perkin-Elmer "spectrum one" spectrometer equipped with an ATR "diamond" apparatus. UV−vis spectra were recorded using a Shimadzu UV-3600 dual-beam grating spectrophotometer with a 1 cm quartz cell. Fluorescence spectra were recorded on a HORIBA Jobin-Yvon fluoromax 4P spectrofluorimeter with a 1 cm quartz cell for solutions or an optical fiber for solids. All fluorescence spectra were corrected. The fluorescence quantum yield (ϕ_{exp}) was calculated from eq 1. Here, *F* denotes the integral of the corrected fluorescence spectrum, *A* is the absorbance at the excitation wavelength, and *n* is the refractive index of the medium. The reference system used was rhodamine 6G in methanol ($\phi_{ref} = 0.78$, $\lambda_{exc} = 488$ nm).

$$\Phi_{exp} = \Phi_{ref} \frac{F\{1 - \exp(-A_{ref} \ln 10)\} n^2}{F_{ref}\{1 - \exp(-A \ln 10)\} n_{ref}^2} \qquad (1)$$

Luminescence lifetimes were measured on a PTI Quanta-Master spectrofluorimeter using TimeMaster software with time-correlated single photon mode coupled to a Stroboscopic system. The excitation source was a thyratron-gated flash lamp filled with nitrogen gas. No filter was used for the excitation. An interference filter centered at 550 nm selected the emission wavelengths. The instrument response function was determined by using a light-scattering solution (LUDOX). Chromatographic purification was conducted using 40−63 μm silica gel. Thin layer chromatography (TLC) was performed on silica gel plates coated with fluorescent indicator. All mixtures of solvents are given in v/v ratio.

General Procedure for the Synthesis of BOD-G$_n$ Compounds (Scheme 1). To a stirred solution of **Acid-G$_n$** (1 equiv) in dry CH₂Cl₂ were added sequentially **B-amino** (10-[4-aminophenyl]-2,8-diethyl-5,5-difluoro-1,3,7,9-tetramethyldipyrrolo[1,2-*c*:2,1-*f*][1,3,2]diazaborinin-4-ium-5-uide), 1-ethyl-3-(3-dimethylaminopropyl)-carbodiimide (EDC·HCl) (3 equiv), and 2,2-dimethylaminopyridine (DMAP) (3 equiv). The reaction mixture was stirred at room temperature until TLC (SiO₂; CH₂Cl₂/MeOH 99:1) indicated no more evolution of the reaction (about 48 h). The reaction mixture was evaporated to dryness, and the residue was dissolved in CH₂Cl₂ (20 mL) and washed with water (3 × 15 mL). The organic layer was dried (MgSO₄) and filtered and the solvent evaporated. The crude product was purified by chromatography on a column packed with silica gel using CH₂Cl₂/MeOH (100/0 to 99.7/0.3) as eluent. Recrystallization from CH₂Cl₂/CH₃CN afforded the desired **BOD-G$_n$** compounds as red powders.

*Compound **BOD-G$_1$***. **BOD-G$_1$** was prepared from **Acid-G$_1$** (0.112 g, 0.07 mmol), **B-amino** (0.033 g, 0.08 mmol), EDC·HCl (0.040 g, 0.21 mmol), DMAP (0.026 g, 0.21 mmol), and CH₂Cl₂ (20 mL) to give 0.080 g (57%) of **BOD-G$_1$** after crystallization from CH₂Cl₂/CH₃CN. ¹H NMR (CDCl₃, 300 MHz): δ (ppm) = 8.59 (t, 1H, arom. H), 8.22−8.08 (m, 8H, arom. H), 8.05 (d, 2H, arom. H), 8.03−7.93 (m, 3H, NH + AB sys.), 7.82 (d, 2H, AB sys.), 7.76−7.57 (m, 12H, arom. H), 7.32 (d, 6H, arom. H), 7.02−6.93 (m, 6H, arom. H), 4.42−4.28 (m, 6H, CO₂CH₂), 4.11−3.94 (m, 6H, CH₂O), 2.53 (s, 6H, CH₃−BOD), 2.30 (q, 4H, CH₂-ethylBOD), 1.89−1.70 (m, 12 H, CO₂CH₂C*H₂* and C*H₂*CH₂O), 1.54−1.23 (m, 42 H, CH₂ + CH₃−BOD), 0.98

Article

Chem. Mater., Vol. 21, No. 17, 2009 3959

(t, 6H, CH$_3$-ethylBOD). ^{13}C NMR (CDCl$_3$, 75 MHz): δ (ppm) = 165.70, 165.09, 164.85, 164.56, 163.88, 163.72, 151.61, 144.86, 136.69, 132.83, 132.64, 132.43, 132.34, 130.00, 129.21, 128.33, 127.68, 127.30, 127.16, 122.55, 121.22, 120.36, 118.86, 114.46, 114.39, 111.01, 68.36, 65.75, 65.63, 30.90, 29.44, 29.40, 29.31, 29.21, 29.08, 28.65, 25.95, 17.07, 14.60, 12.51, 11.93; IR (KBr, cm^{-1}): ν = 2926, 2853, 2227, 1725, 1680, 1605, 1579, 1540, 1511, 1494, 1475, 1422, 1400, 1319, 1259, 1193, 1166, 1113, 1066, 1015, 1006, 980, 918, 878, 844, 819. MALDI-TOF (nature of peak): 1891.4 ([M], 100). Anal. Calcd for C$_{116}$H$_{122}$BF$_2$N$_5$O$_{16}$: C, 73.68; H, 6.50; N, 3.70. Found: C, 73.45; H, 6.25; N, 3.49.

Compound **BOD-G$_2$**. **BOD-G$_2$** was prepared from **Acid-G$_2$** (0.082 g, 0.03 mmol), **B-amino** (0.031 g, 0.08 mmol), EDC·HCl (0.017 g, 0.09 mmol), DMAP (0.011 g, 0.09 mmol), and CH$_2$Cl$_2$ (20 mL) to give 0.052 g (56%) of **BOD-G$_2$** after crystallization from CH$_2$Cl$_2$/CH$_3$CN. ^{1}H NMR (CDCl$_3$, 300 MHz): δ (ppm) = 8.93 (t, 1H, arom. H), 8.63 (t, 2H, arom. H), 8.35 (d, 2H, arom. H), 8.21−8.04 (m, 16H, arom. H), 7.97 (d, 2H, AB sys.), 7.82 (d, 2H, AB sys.), 7.76−7.55 (m, 25 H, arom. H + NH), 7.35−7.22 (m, 10 H, arom. H), 7.03−6.90 (m, 10H, arom. H), 4.36 (t, 10H, CO$_2$CH$_2$), 4.03 (t, 10H, CH$_2$O), 2.53 (s, 6H, CH$_3$−BOD), 2.30 (q, 4H, CH$_2$-ethylBOD), 1.90−1.69 (m, 20 H, CO$_2$CH$_2$C*H$_2$* and C*H$_2$*CH$_2$O), 1.54−1.22 (m, 66H, CH$_2$ + CH$_3$−BOD), 0.98 (t, 6H, CH$_3$-ethylBOD). ^{13}C NMR (CDCl$_3$, 75 MHz): δ (ppm) = 164.87, 164.81, 163.70, 163.06, 151.60, 150.55, 144.85, 136.69, 132.64, 132.54, 132.33, 131.14, 130.02, 129.24, 129.03, 128.32, 127.67, 127.14, 126.99, 122.55, 121.23, 120.34, 118.85, 114.56, 114.37, 111.02, 68.43, 68.34, 65.87, 29.45, 29.41, 29.31, 29.21, 29.08, 28.64, 25.96, 25.94, 17.07, 14.60, 11.93. IR (KBr, cm^{-1}): ν = 2926, 2854, 2226, 1724, 1675, 1603, 1579, 1540, 1510, 1493, 1475, 1439, 1422, 1391, 1315, 1248, 1194, 1163, 1109, 1060, 1018, 1005, 979, 923, 881, 843. MALDI-TOF (nature of peak): 3126.5 ([M], 100). Anal. Calcd for C$_{192}$H$_{192}$BF$_2$N$_7$O$_{30}$: C, 73.76; H, 6.19; N, 3.14. Found: C, 73.42; H, 5.87; N, 2.88.

Compound **BOD-G$_3$**. **BOD-G$_3$** was prepared from **Acid-G$_3$** (0.130 g, 0.025 mmol), **B-amino** (0.012 g, 0.03 mmol), EDC·HCl (0.014 g, 0.075 mmol), DMAP (0.009 g, 0.075 mmol), and CH$_2$Cl$_2$ (40 mL) to give 0.085 g (61%) of **BOD-G$_3$** after crystallization from CH$_2$Cl$_2$/CH$_3$CN. ^{1}H NMR (CDCl$_3$, 300 MHz): δ (ppm) = 8.98−8.94 (m, 3H, arom. H), 8.62 (t, 4H, arom. H), 8.39 (d, 6H, arom. H), 8.16−8.07 (m, 26H, arom. H), 7.97 (d, 2H, AB sys.), 7.81 (d, 2H, AB sys.), 7.75−7.56 (m, 51H, arom.H + NH), 7.35−7.21 (m, 18H, arom. H), 7.02−6.90 (m, 18H, arom. H), 4.35 (t, 18H, CO$_2$CH$_2$), 4.02 (t, 18H, CH$_2$O), 2.53 (s, 6H, CH$_3$− BOD), 2.30 (q, 4H, CH$_2$-ethylBOD), 1.87−1.69 (m, 36H, CO$_2$CH$_2$C*H$_2$* and C*H$_2$*CH$_2$O), 1.52−1.21 (m, 114H, CH$_2$ + CH$_3$−BOD), 0.98 (t, 6H, CH$_3$-ethylBOD). ^{13}C NMR (CDCl$_3$, 75 MHz): δ (ppm) = 164.83, 164.77, 163.68, 151.58, 150.50, 144.82, 136.68, 132.63, 132.32, 128.31, 127.66, 126.96, 122.53, 121.24, 118.83, 114.36, 111.03, 68.33, 65.88, 30.90, 29.44, 29.41, 29.31, 29.21, 29.08, 28.64, 25.96, 25.92, 14.60. IR (KBr, cm^{-1}): ν = 2925, 2853, 2226, 1725, 1678, 1603, 1578, 1538, 1510, 1493, 1474, 1436, 1422, 1392, 1315, 1253, 1196, 1163, 1112, 1064, 1005, 980, 909, 881, 842. MALDI-TOF (nature of peak): 5596.8 ([M], 100). Anal. Calcd for C$_{344}$H$_{332}$BF$_2$N$_{11}$O$_{58}$: C, 73.82; H, 5.98; N, 2.75. Found: C, 73.53; H, 5.77; N, 2.49.